iScience

CellPress
OPEN ACCESS

Article

A dual *SHOX2:GFP; MYH6:mCherry* knockin hESC reporter line for derivation of human SAN-like cells

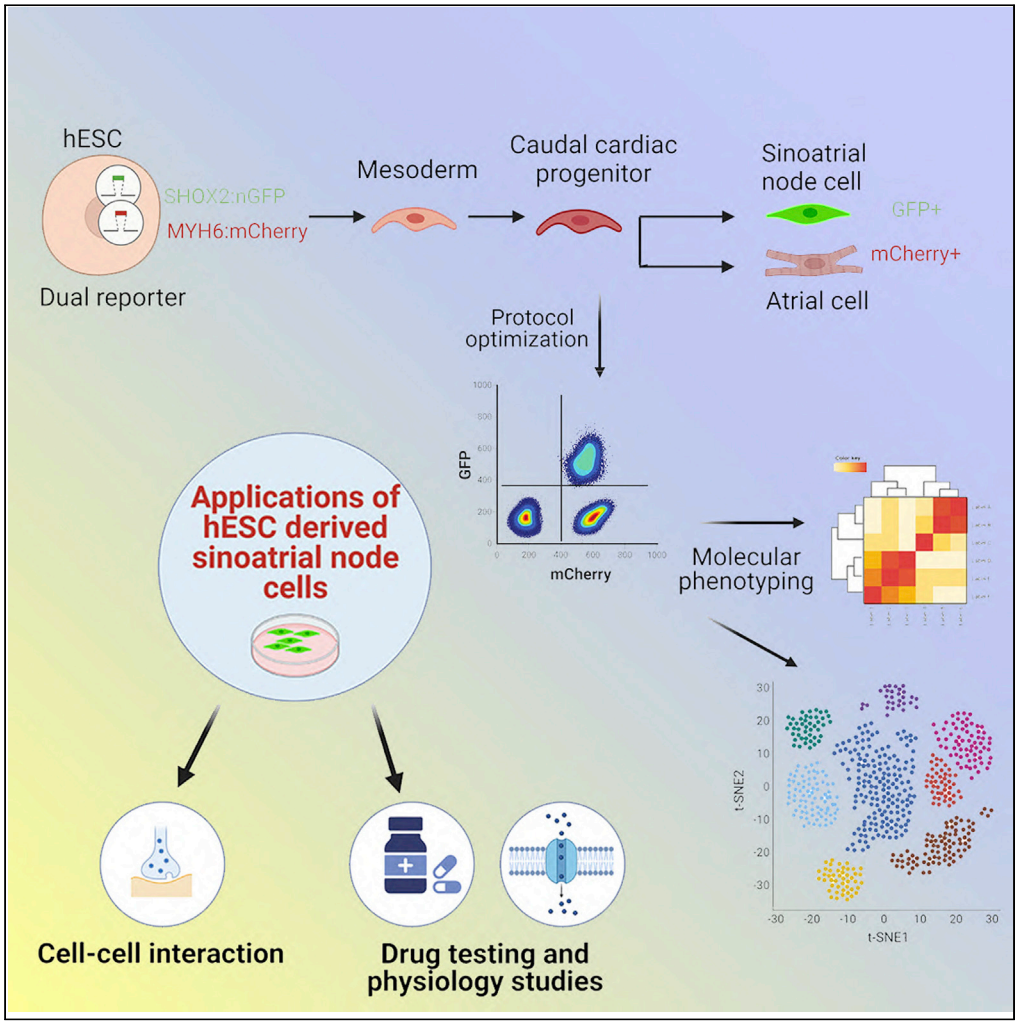

Zaniar Ghazizadeh, Jiajun Zhu, Faranak Fattahi, ..., Geoffrey S. Pitt, Todd Evans, Shuibing Chen

xaniar@gmail.com (Z.G.)
tre2003@med.cornell.edu (T.E.)
shc2034@med.cornell.edu (S.C.)

Highlights

We developed a dual *SHOX2:GFP;MYH6:mCherry* knockin hESC reporter line

An efficient strategy was developed to generate and purify hESC-SAN cells

hESC-SAN cells display molecular and electrophysiological identities of nodal cells

Single-cell RNA sequencing analysis was applied to characterize the hESC-SAN cells

Ghazizadeh et al., iScience *25*, 104153
April 15, 2022
https://doi.org/10.1016/j.isci.2022.104153

iScience

CellPress
OPEN ACCESS

Article

A dual *SHOX2:GFP; MYH6:mCherry* knockin hESC reporter line for derivation of human SAN-like cells

Zaniar Ghazizadeh,[1,11,*] Jiajun Zhu,[1] Faranak Fattahi,[2,3,4] Alice Tang,[1] Xiaolu Sun,[5] Sadaf Amin,[1,12] Su-Yi Tsai,[6] Mona Khalaj,[1] Ting Zhou,[2] Ryan M. Samuel,[3,4] Tuo Zhang,[7] Francis A. Ortega,[8,9] Miriam Gordillo,[1] Dorota Moroziewicz,[10] The NYSCF Global Stem Cell Array® Team,[10] Daniel Paull,[10] Scott A. Noggle,[10] Jenny Zhaoying Xiang,[7] Lorenz Studer,[2] David J. Christini,[9] Geoffrey S. Pitt,[5] Todd Evans,[1,*] and Shuibing Chen[1,13,*]

SUMMARY

The sinoatrial node (SAN) is the primary pacemaker of the heart. The human SAN is poorly understood due to limited primary tissue access and limitations in robust *in vitro* derivation methods. We developed a dual *SHOX2:GFP; MYH6:mCherry* knockin human embryonic stem cell (hESC) reporter line, which allows the identification and purification of SAN-like cells. Using this line, we performed several rounds of chemical screens and developed an efficient strategy to generate and purify hESC-derived SAN-like cells (hESC-SAN). The derived hESC-SAN cells display molecular and electrophysiological characteristics of bona fide nodal cells, which allowed exploration of their transcriptional profile at single-cell level. In sum, our dual reporter system facilitated an effective strategy for deriving human SAN-like cells, which can potentially be used for future disease modeling and drug discovery.

INTRODUCTION

Despite remarkable progress in our understanding of the transcriptional regulation of cardiogenesis and the blueprint that specifies the four-chambered mammalian heart, as well as many of the pathologic processes that lead to cardiac dysfunction, relatively less is known about the specialized network of cells that regulate cardiac rhythmicity, known as the cardiac conduction system (CCS). At the top of the CCS hierarchy is the sinoatrial node (SAN) comprised of SAN cells that generate the electrical impulses triggering each heartbeat. The SAN cells are unique based on their capacity to drive spontaneous electrical activity regulated by autonomic responsiveness. Loss of SAN cells and SAN fibrosis are the major causes of sinus node dysfunction (SND), and there are no cellular or pharmacological therapies to treat such disease. Thus, there is a need to develop strategies to treat patients with CCS defects. Artificial pacemakers and defibrillators can be effective in many cases, and over 200,000 devices are implanted each year in the US (Mond and Proclemer, 2011). However, these treatments can have low efficacy and also cause additional problems, such as pro-arrhythmia side effects, infection, and device malfunction (Holzmeister and Leclercq, 2011; Woods and Olgin, 2014). Devices placed into pediatric patients must be replaced as heart growth proceeds throughout life. Thus, there is a clear and compelling need to develop strategies to derive SAN cells for modeling CCS diseases and potentially for cell replacement therapy.

Human embryonic stem cells (hESCs) and human induced pluripotent stem cells (hiPSCs) provide, in theory, unlimited resources to derive functional human cells. Current progress in the directed differentiation to subtype-specific cardiomyocytes including SAN-like cells has been recently comprehensively reviewed (Zhao et al., 2020b). Some protocols have reported deriving SAN-like cells from hESC/iPSCs through stepwise directed differentiation (Protze et al., 2017b), inhibiting nodal signaling (Yechikov et al., 2020), modulating Wnt signaling (Liang et al., 2020; Ren et al., 2019), or through forced expression of *TBX3* (Zhao et al., 2020a) or *TBX18* (Gorabi et al., 2019), although most of these reports do not use selection, or use an *NKX2.5* negative selection approach to enrich SAN-like cells. Owing to lack of a purification method, it is challenging to determine the efficiency, cellular identity, and function of the derived cells (Kapoor et al.,

[1]Department of Surgery, Weill Cornell Medical College, New York, NY 10065, USA

[2]The Center for Stem Cell Biology, Memorial Sloan Kettering Cancer Center, New York, NY 10065, USA

[3]Department of Cellular and Molecular Pharmacology, University of California, San Francisco, San Francisco, CA 94158, USA

[4]Eli and Edythe Broad Center of Regeneration Medicine and Stem Cell Research, University of California, San Francisco, San Francisco, CA 94143, USA

[5]Cardiovascular Research Institute, Weill Cornell Medicine, New York, NY 10021, USA

[6]Department of Life Science, National Taiwan University, Taipei 10617, Taiwan

[7]Genomic Resource Core Facility, Weill Cornell Medical College, New York, NY 10065, USA

[8]Physiology, Biophysics, and Systems Biology Graduate Program, Weill Cornell Medical College, New York, NY 10065, USA

[9]Department of Physiology & Pharmacology, SUNY Downstate Health Sciences University, Brooklyn, NY 11203, USA

[10]The New York Stem Cell Foundation Research Institute, 619 West 54th Street, 3rd Floor, New York, NY 10019, USA

[11]Present address: Division of Cardiovascular Medicine, Department of Medicine, Stanford University School of

Continued

2013; Protze et al., 2017a). To solve this issue, we created a dual knockin *SHOX2:GFP; MYH6:mCherry* reporter line using CRISPR/Cas9-based gene-targeting techniques to quantify and purify SAN-like cells for developmental studies, purification, disease modeling, and drug discovery.

RESULTS

Generation of human SAN-like cells from hESCs

We sought to develop a protocol that maximizes the generation of pluripotent stem cell-derived SAN pacemaker lineages (PSC-SAN). Based on previous reports (Hoogaars et al., 2007; Ionta et al., 2015; McNally and Svensson, 2009), SAN progenitors are expected to be enriched for expression of key pacemaker transcription factors *TBX3*, *TBX18*, and *SHOX2* (*TTS*). Previously, we engineered murine embryonic stem cell (ESC) lines for conditional expression of GATA4, GATA5, or GATA6, to efficiently generate diverse cardiac cell populations including, nodal, atrial, and ventricular cells (Turbendian et al., 2013). Among these cell lines, GATA5 expression resulted in the highest transcript levels of *TTS* (Figure S1A). We therefore performed an unbiased qRT-PCR-based chemical screen on GATA5-induced progenitors using annotated pathway modulating compounds to identify modulators that further enhance the expression of *TTS* and specification toward pacemaker lineage. Two compounds caused a minimum of 2-fold increase in transcript levels for at least two of the transcription factors (Figure S1B). Both were EGF pathway inhibitors (Figure S1C), suggesting an important role for the EGF pathway in nodal identity, consistent with previous mouse studies (Zhu et al., 2010). Given the association of the SAN with the right atrium, we also focused on the chemicals that increased the expression of atrial rather than ventricular cardiac lineage structural proteins. The screen identified cucurbitacin, a STAT3 inhibitor, that enhances the expression levels of nodal and atrial structural marker *Myh6* (Figure S1D).

These results were next translated into a hESC differentiation protocol, including two additional pathway modulators. Retinoic acid (RA) was included to shift regional identity of cardiac progenitors toward a more caudal phenotype, since pacemaker cells are thought to arise from a more caudal population of cardiac progenitors (Devalla et al., 2015). In addition, an FGF inhibitor was used to augment the expression of *ISL1*, a known regulator of the nodal program in early mouse development (Birket et al., 2015; Liang et al., 2015). Collectively, the full combination (condition 8) of 5 μM EGF inhibitor (Tyrphostin AG490), 0.1 μM STAT3 inhibitor (cucurbitacin), 5 μM FGFR inhibitor (SU5402), and 1 μM RA significantly increased human *TTS* expression levels (Figures 1A, 1B, and S1E).

To quantify and purify SAN-like cells using this directed differentiation protocol, a dual knockin *SHOX2:GFP; MYH6:mCherry* reporter line was created using CRISPR/Cas9-based gene-targeting techniques (Figure S2A). Immunofluorescence and FACS analyses confirmed the success of the protocol for generating putative hPSC-SAN cells, as condition 8 maximized generation of SHOX2:GFP$^+$ cells (Figures 1C, 1D, S2B, and S2C). The sorted GFP$^+$ cells were enriched approximately 4000-fold for *SHOX2* transcript levels compared to GFP$^-$ cells (Figure 1E), and most of the GFP$^+$ cells co-express ISL1 and HCN4 (>95% of cells), proteins closely associated with the development and function of SAN cells (Figure S2D). To further enhance production of GFP$^+$ cells, we considered that SAN development is also controlled epigenetically (Vedantham et al., 2013) and performed an unbiased screen using a library of known epigenetic modulatory compounds. Cells were differentiated using condition 8 with compounds added at day 7 (Figure 1F). After 14 days of differentiation, treatment with the HDAC inhibitor chidamide led to a significant increase in the percentage of GFP$^+$ cells (~50%). Using this directed differentiation protocol (Figure 1G), the GFP$^+$ putative SAN-like cells could be maintained at this level for 30–40 days post differentiation, and without reducing the total cell number, demonstrated by both flow cytometry and immunostaining at day 30 (Figures 1H and S2E). We also differentiated the SHOX2:GFP; MYH6-mCherry reporter line using a standard ventricular cardiomyocyte differentiation protocol (Tsai et al., 2020), and very few SHOX2-GFP$^+$ cells were detected (Figure S2F). Additionally, we performed staining for MYL2, a ventricular cardiomyocyte marker (Luo et al., 2021), and NR2F2, a marker expressed in both atrium and SAN (Burkhard and Bakkers, 2018; Hoffmann et al., 2021). 42.2 ± 7.8% of MYH6:mCherry$^+$ cells are NR2F2$^+$SHOX2-GFP$^-$, suggesting that the protocol generates this level of atrial-like cells in the unpurified population. No MYL2 expression was detected using the current differentiation protocol (Figures S2G and S2H), suggesting that ventricular cardiomyocytes are not present. This result is expected since the protocol was designed to bias away from ventricular cardiomyocyte fate. Given the potential application of pluripotent stem cell-derived nodal cells in disease modeling, we set out to validate the platform in iPSCs. We differentiated two additional (non-reporter) iPSC lines using the same protocol. Owing to the lack of a

Medicine, Stanford, CA 94305, USA

[12]Present address: Helen and Robert Appel Alzheimer's Disease Research Institute, Brain and Mind Research Institute, Weill Cornell Medicine, New York, NY 10021, USA

[13]Lead contact

*Correspondence: xaniar@gmail.com (Z.G.), tre2003@med.cornell.edu (T.E.), shc2034@med.cornell.edu (S.C.)

https://doi.org/10.1016/j.isci.2022.104153

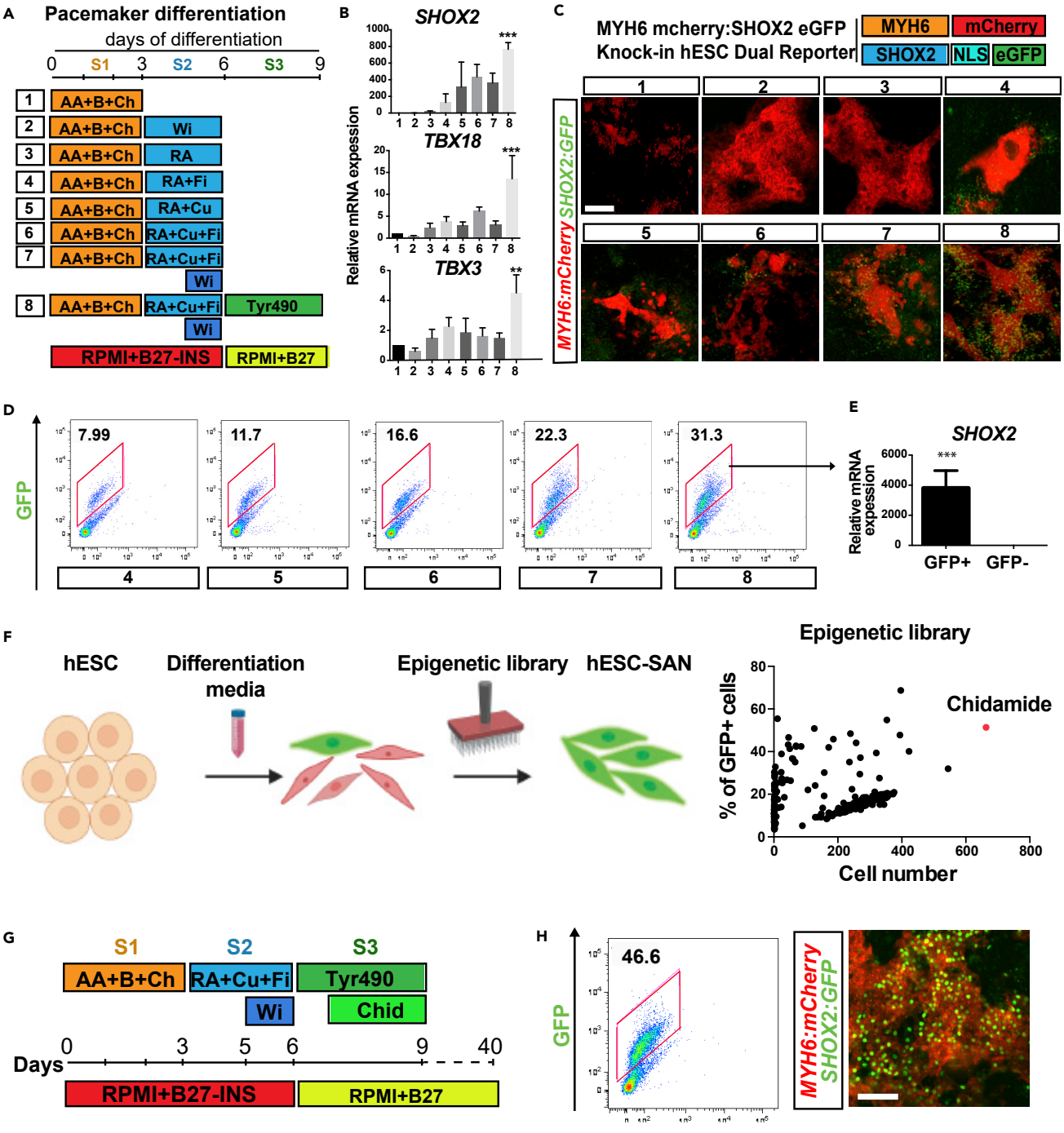

Figure 1. Generation of human SAN-like cells from hESCs

(A) Schematic representation of the differentiation protocols 1–8. The protocol involves three stages (S1, S2, and S3) during the first 9 days of directed differentiation.

(B–D) Quantitative PCR (B), live fluorescence images (C), and FACS plots (D) of the day 30 cells derived from the *SHOX2:GFP;MYH6:mCherry* H9 line using the corresponding differentiation protocols (n = at least 3 biological replicates for each condition). For quantitative PCR data, fold changes were normalized to protocol #1. p values calculated using ordinary one-way ANOVA with Fisher's test (**p < 0.01, ***p < *0.001*). Data are represented as mean ± SEM. The x axis in panel D is side scatter.

(E) Quantitative PCR analysis for *SHOX2* transcriptional expression of GFP^{+} cells purified after sorting. n = 3 biological replicates. p value calculated by unpaired two-tailed Student's t-test ***p < *0.001*. Data are represented as mean ± SEM, and normalized to GFP-negative population.

(F) Schematic and results of the epigenetic library chemical screen.

Figure 1. *Continued*

(G) Schematic of the final differentiation protocol.

(H) Immunofluorescence image and FACS plot of day 30 cells derived using the protocol described in (G), Scale bar = 100 μm. AA: Activin A, B: BMP4, Ch: CHIR99021, Wi: Wnt inhibitor, RA: Retinoic Acid, Fi: FGF inhibitor, Cu: cucurbitacin, Tyr490: tyrphostin AG 490.

See also Figures S1 and S2.

commercially available reliable SHOX2 antibody, the differentiated cell population was stained for expression of ISL1 (Figure S2I), a marker that overlaps significantly with SHOX2:GFP in hESC-SAN cells (Figure S2C). The percentage of ISL1$^+$ cells was comparable with the percentage of ISL1$^+$ cells generated using the dual reporter hESC line, suggesting that this differentiation protocol can be applied for multiple hESC/iPSC lines.

Transcriptome profiling of hESC-SAN cells

To further validate the nodal identity of the SHOX2:GFP$^+$ cells, the GFP$^+$ versus mCherry$^+$ (GFP$^-$) populations were sorted at day 25 or day 40 of differentiation and compared by RNA-seq profiling. Owing to the lack of RNA-seq data profiling purified human SAN tissue, hESC-derived SAN cells were compared with profiles generated from murine SAN and right atrial (representing mostly atrial myocardium) tissues (GSE65658) (Vedantham et al., 2015). The data were analyzed by hierarchical clustering alongside RNA-seq databases generated using HCN4:GFP$^+$ cells from dissected murine SAN tissue and GFP$^-$ cells from adjacent right atrial tissue. Whether the clustering analysis used whole transcriptomic data (Figure 2A) or selected datasets for genes encoding ion channels, structural proteins, metabolic proteins, or growth factors (Figure 2B), the GFP$^+$ and mCherry$^+$ cell profiles clustered with SAN and atrial cardiomyocyte profiles, respectively. The phenotypes were further confirmed by gene set enrichment analyses: the geneset representing genes with levels enhanced 10-fold in SAN vs atrial cells were highly enriched in GFP$^+$ cells while those that have levels enhanced 10-fold in atrial vs SAN cells were highly enriched in mCherry$^+$ cells (Figure 2C).

Functional characterization of hESC-SAN cells

We maintained differentiated cells for up to 60 days and evaluated gene expression patterns. At day 30, SHOX2:GFP$^+$ cells stained positive by immuno-fluorescence for HCN4, ISL1, and TBX5 (Figure 3A). By day 60, there was increased expression levels for channels related to pacemaker activity, including $Ca_V3.1$, $Ca_V1.3$, and Cx30.2 (Figure 3A). Expression of these nodal markers is not increased in mCherry+; GFP- cardiomyocytes (Figure S3A). Transcript levels of pacemaker markers *TBX3*, *TBX18*, *ISL1*, and *HCN4* were significantly higher in SHOX2:GFP$^+$; MYH6:mCherry$^+$ cells compared to SHOX2:GFP$^-$; MYH6:mCherry$^+$ cells. On the other hand, atrial cardiomyocyte marker *Nppa* was lower in SHOX2:GFP$^+$; MYH6:mCherry$^+$ cells compared to SHOX2:GFP$^-$; MYH6:mCherry$^+$ cells (Figure 3B). There was no significant difference in *NKX2.5* expression levels comparing these two populations until day 45 (Figure 3B). This is in agreement with previous *in vitro* and *in vivo* studies showing that NKX2.5 and SHOX2 are co-expressed during the early stages of mouse development (Goodyer et al., 2019) and differentiating embryoid bodies (Ye et al., 2015). At day 45, the expression level of *NKX2.5* in SHOX2:GFP$^+$ cells is significantly lower than in MYH6:mCherry$^+$ cells (Figure 3B), which is consistent with suppression of *NKX2.5* by SHOX2 (Espinoza-Lewis et al., 2009). These results highlight the importance of development of strategies for direct isolation and characterization of SAN cells using nodal-specific markers.

A major function of the SAN is to regulate heart rhythm under the control of autonomic neurons (AN). ESC-derived cardiomyocytes show poor connectivity with ESC-derived AN (Oh et al., 2016). We probed the functionality of *in-vitro*-derived hPSC-SAN cells by assessing connectivity with AN (Figure 3C). For connectivity studies, an optogenetic reporter line was used to facilitate light-induced control of neural activity (Fattahi et al., 2016). AN were derived as previously described (Tchieu et al., 2017; Zeltner et al., 2016) from a hESC line expressing enhanced yellow fluorescent protein (eYFP)-tagged channelrhodopsin-2 (ChR2) under control of the human synapsin promoter. Co-culture of day 25 hPSC-SAN cells with these AN resulted in physical connection between SAN cells and AN, as shown by increased expression of synapsin, and junctional morphology indicated by electron microscopy (Figure 3D). Furthermore, the co-culture platform resulted in increased maturation of AN as shown by increased adrenaline levels in supernatant compared to AN co-cultured with hESC-derived

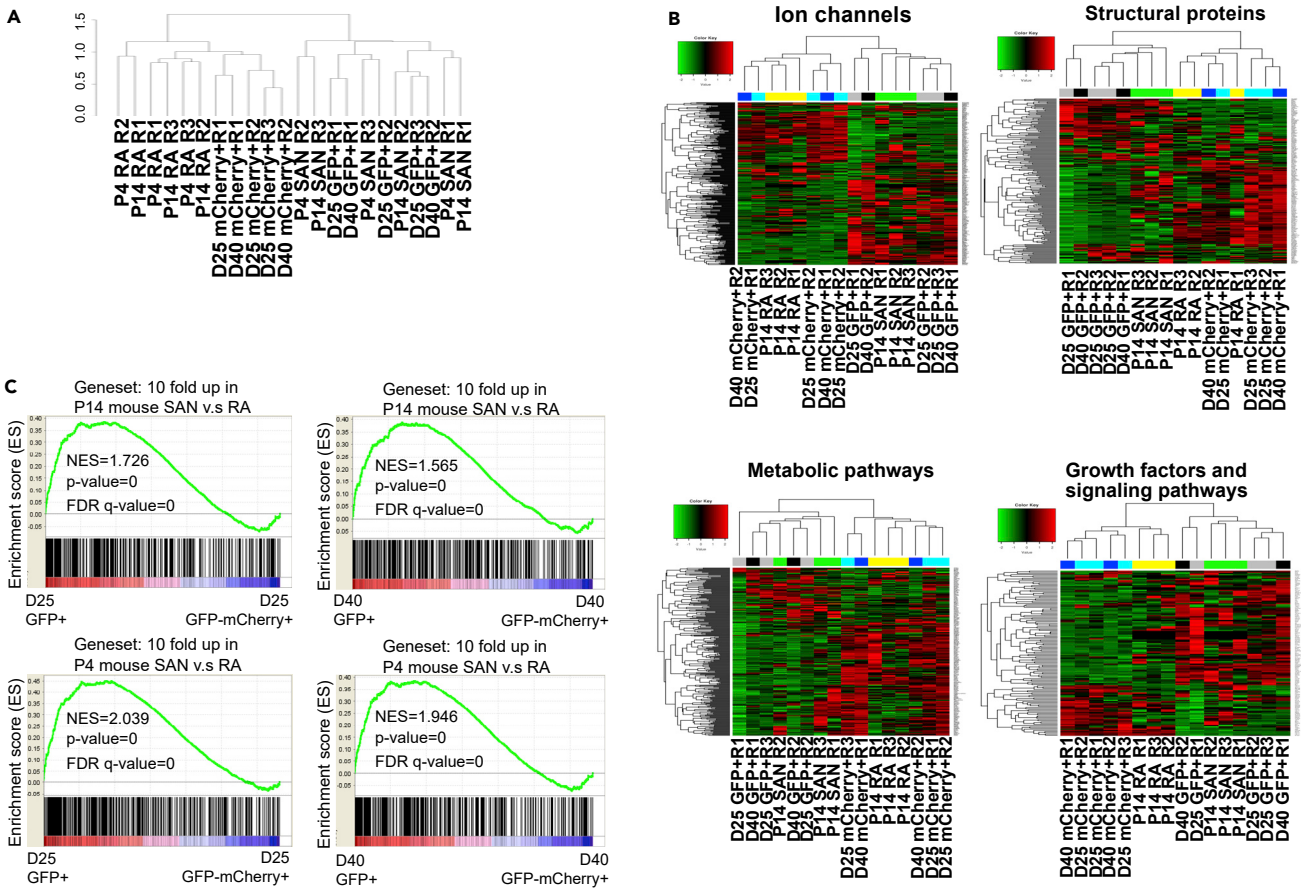

Figure 2. Transcriptome profiling of hESC-SAN cells

(A and B) Hierarchical clustering (A) and heatmap (B) of transcriptional profiling in GFP$^+$ cells and mCherry$^+$ cells purified as described in (S2B) compared to murine SAN or murine right atrial (RA) profiles (GSE65658).

(C) Gene set enrichment analysis in purified GFP$^+$ cells and GFP$^-$mCherry$^+$ cells. Murine sinoatrial and atrial tissues (GSE65658) were used as controls. RA: murine right atrial sample; SAN: murine sinoatrial node sample. R1, R2, and R3 represent independent replicates and the labels P4 and P14 refer to post-natal day 4 and day 14 samples. The human SAN-like cell profiles always cluster with murine SAN profiles, while human CM cell profiles always cluster with murine right atrium myocardium profiles.

ventricular-like cardiomyocytes (hESC-V cells) (Figures 3E and S3B). Light-activated contractions in SAN cells further validated the connectivity (Video S1).

One key functional property of a nodal cell is its characteristic action potential with fast spontaneous firing rates and slow maximum upstroke velocities (<30 V/s). SHOX2:GFP$^+$ cells generated from the differentiation protocol at day 30 were sorted and patch-clamping experiments showed 8 out of 10 demonstrated the characteristic electrophysiologic phenotype of nodal cells, distinct from hPSC-V cells (Figure 3F). In addition, the beating rate of hESC-SAN cells is significantly higher than hESC-V cells (Figure 3G). The hPSC-SAN cells showed spontaneous firing characteristic of pacemaker action potential (Figure 3H). We tested the hPSC-derived pacemaker cells for the presence of I_h current by patch clamp and found the expected inward current that increased with larger hyperpolarizing steps in 5 of 5 cells tested (example traces and I-V curve of hESC-SAN in Figure 3I). In comparison, hESC-derived ventricular cardiomyocytes (example traces of hESC-V in Figure 3I) lacked I_h current, and instead exhibited only a leaky current with the identical hyperpolarizing voltage protocol. To further test functionality of nodal-specific ion channels in hPSC-SAN cells, we used rate-modifying drugs and explored their effect on these cells. Ivabradine, a specific HCN4 channel modulator (Postea and Biel, 2011), has been shown to slow SAN activity. A Ca^{2+}-flux assay was used to record the baseline calcium activity of hESC-SAN or hESC-V cells, which were then treated with 1 μM ivabradine and recordings taken after 5 min. While no significant difference was observed in

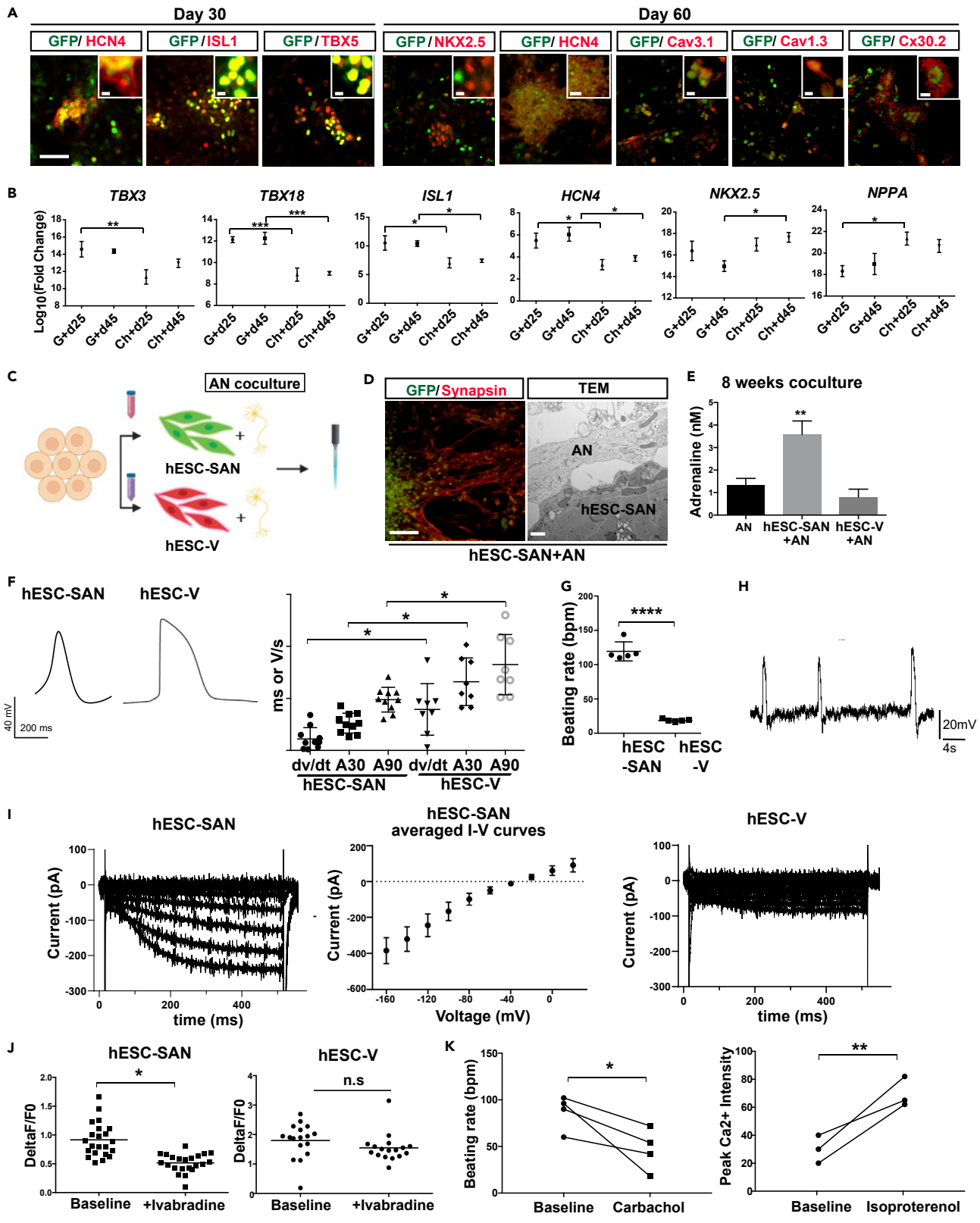
A
Day 30
Day 60
GFP/ HCN4
GFP/ ISL1
GFP/ TBX5
GFP/ NKX2.5
GFP/ HCN4
GFP/ Cav3.1
GFP/ Cav1.3
GFP/ Cx30.2
B
TBX3
TBX18
ISL1
HCN4
NKX2.5
NPPA
Log10 (Fold Change)
G+d25
G+d45
Ch+d25
Ch+d45
C
AN coculture
hESC-SAN
hESC-V
D
GFP/ Synapsin
TEM
AN
hESC-SAN
hESC-SAN+AN
E
8 weeks coculture
Adrenaline (nM)
AN
hESC-SAN +AN
hESC-V +AN
F
hESC-SAN
hESC-V
40 mV
200 ms
ms or V/s
dv/dt A30 A90 dv/dt A30 A90
hESC-SAN
hESC-V
G
Beating rate (bpm)
hESC -SAN
hESC -V
H
20mV
4s
I
hESC-SAN
hESC-SAN averaged I-V curves
hESC-V
Current (pA)
time (ms)
Voltage (mV)
J
hESC-SAN
hESC-V
DeltaF/F0
n.s
Baseline
+Ivabradine
K
Beating rate (bpm)
Baseline
Carbachol
Peak Ca2+ Intensity
Baseline
Isoproterenol

Figure 3. Functional characterization of hESC-SAN cells

(A) Immunofluorescent co-staining of GFP with pacemaker-associated transcription factors (ISL1, TBX5, and NKX2.5) and ion channels (HCN4, Cav3.1, Cav1.3, and Cx30.2) in cells differentiated to day 30 or day 60. Scale bar = 200 μm.

(B) qRT-PCR analysis using samples from GFP^+ (G+) or $mCherry^+$ (Ch+) cells at day 25 or day 45. n = 3 biological replicates. Fold change was normalized to undifferentiated hESCs. p values calculated by one-way ANOVA with Fisher's test (*p < 0.05, **p < 0.01, ***p < *0.001*). Data are represented as mean ± SEM.

(C) Schematic for co-culture of hESC-derived ANs expressing eYFP-channelrhodopsin-2 with either hESC-SAN or hESC-V.

(D) Representative immunofluorescence (left panel) and electron microscopy images (right panel) of hESC-AN and hESC-SAN after 12 weeks of co-culture. Scale bar: 100 μm (left panel) and 1 μm (right panel).

(E) Basal release of catecholamine was analyzed using an ELISA kit for AN alone, AN + hESC-SAN and AN + hESC-V conditions after 8 weeks of co-culture. n = 3 biological replicates. p values calculated by one-way ANOVA (**p < *0.01*). Data are represented as mean ± SEM.

(F) Representative image of averaged action potentials recorded by perforated patch clamp from individual hESC-SAN (left) and hESC-V (right) cells and distribution of dV/dt_{max}, APD30, and APD90 recorded used day 30 cells. p values calculated by one-way ANOVA used to compare means (*p < 0.05). Data are represented as mean ± SEM.

(G) Beating rate of hESC-SAN and hESC-V cells. p values calculated by unpaired two-tailed Student's t-test ****p < *0.0001*. Data are represented as mean ± SEM. (H) Spontaneous firing of hESC-SAN cells. Note that for these experiments, cells were replated as single cells on cover slips and they were maintained in physiological buffers (rather than their optimal cell culture media). Cells are manipulated for up to an hour at room temperature, during which time the beating rate decreases substantially (compared to conditions in G).

(I) I_h current measurements in hESC-SAN or hESC-V cells by patch clamp. Left: Example traces of hESC-SAN cells; Middle: Averaged I-V curves; Right: Example traces of hESC-V cells. (n = 5 biological replicates).

(J) Quantitative analysis of day 30 hESC-SAN function in response to 1 μM ivabradine. Fold change in calcium transient amplitude (deltaF/F0) of hESC-SAN or hESC-V cells before and after treatment with ivabradine (n = 22 biological replicates for hESC-SAN and n = 17 biological replicates for hESC-V). Unpaired two-tailed Student's t-test was used to compare means (*p < 0.05). Each dot represents data measured from independent cells.

(K) Quantitative analysis of day 30 hESC-SAN function in response to 1 μM isoproterenol and 5 μM carbachol. p values calculated by unpaired two-tailed Student's t-test *p < 0.05, **p < *0.01*. Data are represented as mean ± SEM.

See also Figure S3A and Video S1.

hESC-V cell cultures, a significant reduction was observed in Ca^{2+}-flux activity in the hESC-SAN cells (Figure 3J). A Ca^{2+}-flux assay was also used to monitor the response of hESC-SAN cells to 1 μM isoproterenol or 5 μM carbachol treatment (Figure 3K). Carbachol treatment had negative chronotropic and isoproterenol had positive inotropic effects on hESC-SAN cells. Therefore, based on multiple criteria, including gene expression profiles, AN connectivity, electrophysiological characteristics, and drug sensitivity, the hESC-SAN cells recapitulate expected features of human nodal pacemaker cells.

Single-cell RNA sequencing analysis of differentiated hESC-SAN and hESC-V cells

The hPSC-SAN cells were analyzed in a single-cell RNAseq experiment to explore heterogeneity of the cell population and identify lineage-restricted transcriptome features. For this purpose, SHOX2:GFP^+ cells were sorted from the pacemaker differentiation culture, and MYH6:$mCherry^+$ cells were sorted following cardiomyocyte directed differentiation to generate a ventricular-like population (hESC-V). After pooled sequencing, tSNE plots (Figure 4A) clustered cells with similar gene expression patterns. Cluster analysis using global gene expression values classified the cells into three groups including high-SHOX2, no-SHOX2, and a smaller cluster of mixed-SHOX2 cells. The mixed-SHOX2 population contains both GFP^+ and $mCherry^+$ cells (Figure S3C). Because cardiac markers are not highly expressed in the mixed-SHOX2 population, these cells might represent non-cardiac $SHOX2^+$ cells (Figure 4B). We therefore focused on high-SHOX2 and no-SHOX2 cells for further analysis. Principal component analysis (PCA, Figure 4C) confirmed that high-SHOX2 and no-SHOX2 cells are two distinct populations (Figure 4C).

High-SHOX2 cells significantly expressed transcripts encoding structural proteins *TPM1, MYL7, MYH6, MYL6, ACTA2, DSTN, ACTC1, NEXN, NEBL, MYH11,* and *MYLK* (Figure 4D). The role in SAN physiology for some of these proteins including MYLK, MYH11, and ACTA2 is unknown, although they were also reported to be present in the murine SA node (Vedantham et al., 2015). Notable structural protein genes expressed in the no-SHOX2 cell population include *TTN, TPM1, MYL7, MYH6,* and *ACTC1* (Figure 4D). The high-SHOX2 cell population was relatively homogenous in expression of transcripts for the key ion channel *HCN4* and transcriptional regulator *ISL1*, while no-SHOX2 cells showed heterogeneity in the expression levels of these two genes (Figure 4E). *PITX2c*, a gene responsible for suppression of the SAN program in atrial cells (Wang et al., 2010), was highly expressed in the no-SHOX2 cells while expressed at very low relative levels in the high-SHOX2 cells. The presence of *IRX4* transcripts in the no-SHOX2 cells (and absence in the high-SHOX2 cells) confirms the ventricular identity of the former (Figure 4F). The high-SHOX2 cell population had lower but detectable *NKX2.5* expression levels, and was also associated with relatively higher

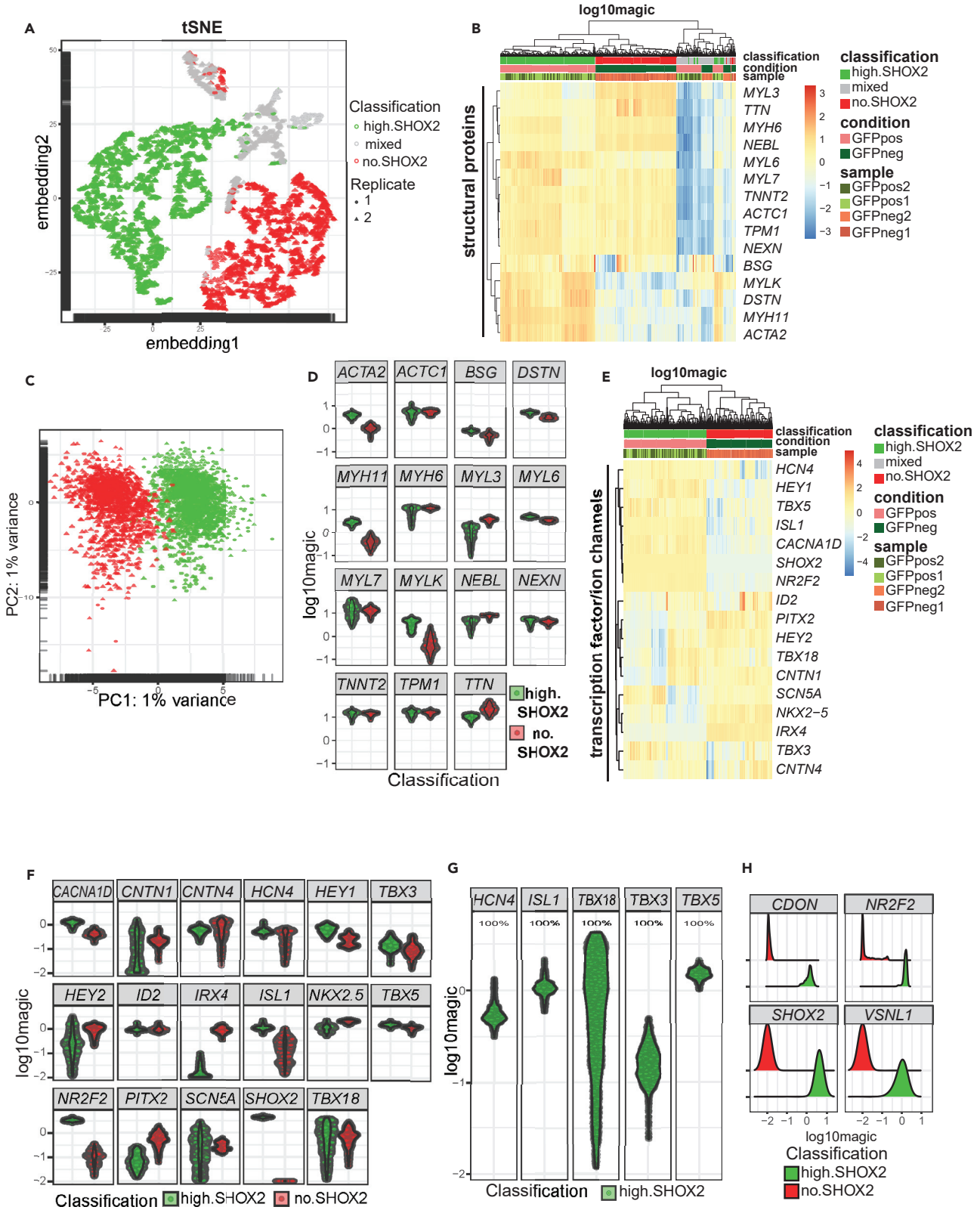
A
tSNE
embedding2
embedding1
Classification
high.SHOX2
mixed
no.SHOX2
Replicate
1
2
B
log10magic
classification
condition
sample
structural proteins
MYL3
TTN
MYH6
NEBL
MYL6
MYL7
TNNT2
ACTC1
TPM1
NEXN
BSG
MYLK
DSTN
MYH11
ACTA2
classification
high.SHOX2
mixed
no.SHOX2
condition
GFPpos
GFPneg
sample
GFPpos2
GFPpos1
GFPneg2
GFPneg1
C
PC2: 1% variance
PC1: 1% variance
D
ACTA2
ACTC1
BSG
DSTN
MYH11
MYH6
MYL3
MYL6
MYL7
MYLK
NEBL
NEXN
TNNT2
TPM1
TTN
log10magic
high. SHOX2
no. SHOX2
Classification
E
log10magic
classification
condition
sample
transcription factor/ion channels
HCN4
HEY1
TBX5
ISL1
CACNA1D
SHOX2
NR2F2
ID2
PITX2
HEY2
TBX18
CNTN1
SCN5A
NKX2−5
IRX4
TBX3
CNTN4
classification
high.SHOX2
mixed
no.SHOX2
condition
GFPpos
GFPneg
sample
GFPpos2
GFPpos1
GFPneg2
GFPneg1
F
CACNA1D
CNTN1
CNTN4
HCN4
HEY1
TBX3
HEY2
ID2
IRX4
ISL1
NKX2.5
TBX5
NR2F2
PITX2
SCN5A
SHOX2
TBX18
log10magic
Classification
high.SHOX2
no.SHOX2
G
HCN4
ISL1
TBX18
TBX3
TBX5
100%
log10magic
Classification
high.SHOX2
H
CDON
NR2F2
SHOX2
VSNL1
log10magic
Classification
high.SHOX2
no.SHOX2

Figure 4. Single-cell RNA sequencing analysis of differentiated hESC-SAN and hESC-V cells

(A) t-SNE plots colored according to the cell populations.

(B) Heatmap based on structural protein expression showing the clustering of the high-SHOX2, mixed-, and no- SHOX2 cells.

(C) PCA plot of high-SHOX2 and no-SHOX2 cells.

(D) Jitter plots based on structural protein expression of high-SHOX2 and no-SHOX2 cells.

(E and F) Heatmap (E) and jitter plots (F) based on expression of key transcription factors and ion channels in high-SHOX2 and no-SHOX2 cells.

(G and H) Jitter plots for the expression of *HCN4, ISL1, TBX3, TBX5,* and *TBX18* (G) and jitter plots for the expression of *SHOX2, CDON, NR2F2,* and *VSNL1,* (H) in the high-SHOX2 and no-SHOX2 cells.

See also Figure S3B.

levels of *HEY1* and *ID2* transcripts, consistent with an SA nodal identity rather than an AV node (Hoogaars et al., 2007; Horsthuis et al., 2009; McNally and Svensson, 2009). Consistent with previous studies, *CACNA1D* (encoding $Ca_V1.3$), which is necessary for the pace-making activity of nodal cells (Torrente et al., 2016), was relatively enriched in high-SHOX2 cells. Among contactin (CNTN) isoforms, *CNTN4* transcripts were relatively more abundant in the high-SHOX2 cell population, compared to variable expression levels of *CNTN1*.

Consistent with the heat maps, jitter plots show that the high-SHOX2 population showed relatively homogenous expression of *HCN4, ISL1, TBX5,* and *TBX3* genes compared to *TBX18* (Figure 4G). Previous murine developmental studies suggested that the *TBX18* expression pattern might determine the identity of different parts of the SA node, including head or tail (Wiese et al., 2009). The single-cell sequencing data indicate that the *in vitro* generated hPSC-SAN cells recapitulate a spectrum of *TBX18* expression patterns, and therefore may represent multiple segments of the SA node. Another key calcium regulator identified in high-SHOX2 cells was *VSNL1* (Figure 4H). Given the importance of SAN action potential in regulation of rate and rhythm, we further focused on whether this gene is expressed in adult tissue. Single-cell analysis from adult tissue biopsies proved that *VSNL1* is co-expressed with HCN4 and CACNA1D in the adult tissue (Figures S3C and S3D). Previously, a number of transcription factors or calcium channels, such as SMOC2, BMP2, GFRA2, and NOTCH3, were proposed to be enriched in the murine SA node (van Eif et al., 2019). However, none of these genes were co-expressed with HCN4 in adult heart tissue single-cell analysis, suggesting the need for further studies to elucidate their role in human nodal physiology (Figure S3D).

DISCUSSION

This study describes an efficient strategy to derive and purify SAN-like cells from hPSCs. The ability to generate human SAN-like cells *in vitro* can facilitate study of genetic and iatrogenic arrhythmias and may eventually allow scaled production and transplantation as biological pacemakers. Previous efforts focused on *in vivo* direct conversion or an NKX2.5 negative selection approach to obtain nodal-like cells. However, due to lack of a purification method, the studies were limited in characterization and validation of nodal identity for the cells at cellular and molecular levels (Kapoor et al., 2013; Protze et al., 2017a). Our reporter strategy enabled direct visualization and standardized *in vitro* assays for developmental studies, purification, and drug discovery (Birket et al., 2015; Cingolani et al., 2017; Kapoor et al., 2013). We demonstrate functionality of the *in-vitro*-derived cells through several methods including global gene expression analysis, cell-type-specific expression profiling, and electrophysiological mapping. While the ESC-derived SAN-like cell profiles clustered with murine SAN tissue profiles rather than atrial myocardium profiles, it will be important in future experiments to compare directly to human tissues. Notably these cells were able to make functional connectivity with autonomic neurons, enabling studying synaptic activity and neurotransmitter release. Furthermore, the ability to directly purify these cells led to single-cell analysis of an enriched population of SAN cells. This showed a spectral expression of TBX18 and TBX3, similar to the developing nodal cells in addition to identification of previously unknown genes involved in nodal cell physiology. Therefore, the precise isolation and expansion of these cells can pave the way for better understanding of cell and non-cell autonomous processes involved in nodal tissue biology in regulating rate and rhythm in conjunction with the autonomic nervous system. The human SAN-like cells derived here can be potentially used for cardiac nodal disease modeling and drug screens.

Limitations of the study

Although scRNA-seq analysis of hESC-derived SAN-like cells identified some previously unknown markers for SAN, additional work is needed to validate the expression and determine the biological function of the

identified markers. While the cell profiles did not identify specific SAN-like cell subsets, the broad range of expression for some key transcription factors such as TBX18 might indicate heterogeneity, and it will be of interest to determine if this relates to endogenous patterning of the natural SAN. The dual reporter line will provide a powerful tool to study human SAN cells. However, additional purification and maturation strategies will be needed to enrich the SAN-like cells from non-reporter lines and explore potential use in regenerative therapy.

STAR★METHODS

Detailed methods are provided in the online version of this paper and include the following:

- KEY RESOURCES TABLE
- RESOURCE AVAILABILITY
  - Lead contact
  - Materials availability
  - Data and code availability
- EXPERIMENTAL MODEL AND SUBJECT DETAILS
  - Cell lines
- METHOD DETAILS
  - Sinoatrial and ventricular myocyte induction
  - FACS and immuno-fluorescence
  - Gene expression analysis
  - Generation of the SHOX2:GFP; MYH6:mCherry dual hESC reporter line
  - Bulk RNA sequencing
  - Single cell RNA sequencing
  - Adult heart single cell analysis
  - Calcium imaging
  - Cellular electrophysiology and characterization
  - Chemical screen
- QUANTIFICATION AND STATISTICAL ANALYSIS

SUPPLEMENTAL INFORMATION

Supplemental information can be found online at https://doi.org/10.1016/j.isci.2022.104153.

ACKNOWLEDGMENTS

This work was supported by the American Heart Association (18CSA34080171, S.C., T.E.), Department of Surgery, Weill Cornell Medicine (T.E., S.C.), Tri-Institutional Stem Cell Institute (2021-026, S.C.), NIDDK (R01DK130454, R01DK119667-02S1, S.C.), NHLBI (R01HL151190, R01HL160089, G.S.P.). S.C is supported as Irma Hirschl Trust Research Award Scholars. T.E. is supported by an Outstanding Investigator Award (R35 HL135778). We thank Dr. Friederike Dundar for her help on single-cell RNA-seq analysis.

AUTHOR CONTRIBUTIONS

S.C., T.E., and L.S. conceived and designed the experiments. Z.G., J.Z., F.F., A.T., S.A., S.T., M.K., T.Z., and M.G. performed experiments. X.S., F.A.O., D.C., and G.S.P. performed electrophysiology experiments. R.M.S., T.Z., and J.Z.X. performed the bioinformatics analyses.

DECLARATION OF INTERESTS

T.E. and S.C. are founding owners of OncoBeat, LLC. A patent has been filled for "Compositions and methods for generation of sinoatrial node-like cells and their use in drug discovery".

Received: September 20, 2021
Revised: January 25, 2022
Accepted: March 22, 2022
Published: April 15, 2022

REFERENCES

Birket, M.J., Ribeiro, M.C., Verkerk, A.O., Ward, D., Leitoguinho, A.R., den Hartogh, S.C., Orlova, V.V., Devalla, H.D., Schwach, V., Bellin, M., et al. (2015). Expansion and patterning of cardiovascular progenitors derived from human pluripotent stem cells. Nat. Biotechnol. *33*, 970–979.

Burkhard, S.B., and Bakkers, J. (2018). Spatially resolved RNA-sequencing of the embryonic heart identifies a role for Wnt/β-catenin signaling in autonomic control of heart rate. Elife *7*, e31515.

Butler, A., Hoffman, P., Smibert, P., Papalexi, E., and Satija, R. (2018). Integrating single-cell transcriptomic data across different conditions, technologies, and species. Nat. Biotechnol. *36*, 411–420. https://doi.org/10.1038/nbt.4096.

Cingolani, E., Goldhaber, J.I., and Marban, E. (2017). Next-generation pacemakers: from small devices to biological pacemakers. Nat. Rev. Cardiol. *15*, 139–150.

Cong, L., Ran, F.A., Cox, D., Lin, S., Barretto, R., Habib, N., Hsu, P.D., Wu, X., Jiang, W., Marraffini, L.A., et al. (2013). Multiplex genome engineering using CRISPR/Cas systems. Science *339*, 819–823.

Devalla, H.D., Schwach, V., Ford, J.W., Milnes, J.T., El-Haou, S., Jackson, C., Gkatzis, K., Elliott, D.A., Chuva de Sousa Lopes, S.M., Mummery, C.L., et al. (2015). Atrial-like cardiomyocytes from human pluripotent stem cells are a robust preclinical model for assessing atrial-selective pharmacology. EMBO Mol. Med. *7*, 394–410.

Dobin, A., Davis, C.A., Schlesinger, F., Drenkow, J., Zaleski, C., Jha, S., Batut, P., Chaisson, M., and Gingeras, T.R. (2013). STAR: ultrafast universal RNA-seq aligner. Bioinformatics *29*, 15–21.

Espinoza-Lewis, R.A., Yu, L., He, F., Liu, H., Tang, R., Shi, J., Sun, X., Martin, J.F., Wang, D., Yang, J., et al. (2009). Shox2 is essential for the differentiation of cardiac pacemaker cells by repressing Nkx2-5. Dev. Biol. *327*, 376–385.

Fattahi, F., Steinbeck, J.A., Kriks, S., Tchieu, J., Zimmer, B., Kishinevsky, S., Zeltner, N., Mica, Y., El-Nachef, W., Zhao, H., et al. (2016). Deriving human ENS lineages for cell therapy and drug discovery in Hirschsprung disease. Nature *531*, 105–109.

Goodyer, W.R., Beyersdorf, B.M., Paik, D.T., Tian, L., Li, G., Buikema, J.W., Chirikian, O., Choi, S., Venkatraman, S., Adams, E.L., et al. (2019). Transcriptomic profiling of the developing cardiac conduction system at single-cell resolution. Circ. Res. *125*, 379–397.

Gorabi, A.M., Hajighasemi, S., Tafti, H.A., Atashi, A., Soleimani, M., Aghdami, N., Saeid, A.K., Khori, V., Panahi, Y., and Sahebkar, A. (2019). TBX18 transcription factor overexpression in human-induced pluripotent stem cells increases their differentiation into pacemaker-like cells. J. Cell Physiol. *234*, 1534–1546.

Hoffmann, S., Schmitteckert, S., Raedecke, K., Rheinert, D., Diebold, S., Roeth, R., Weiss, B., Granzow, M., Niesler, B., Griesbeck, A., et al. (2021). Network-driven discovery yields new insight into Shox2-dependent cardiac rhythm control. Biochim. Biophys. Acta (Bba) - Gene Regul. Mech. *1864*, 194702.

Holzmeister, J., and Leclercq, C. (2011). Implantable cardioverter defibrillators and cardiac resynchronisation therapy. Lancet *378*, 722–730.

Hoogaars, W.M., Engel, A., Brons, J.F., Verkerk, A.O., de Lange, F.J., Wong, L.Y., Bakker, M.L., Clout, D.E., Wakker, V., Barnett, P., et al. (2007). Tbx3 controls the sinoatrial node gene program and imposes pacemaker function on the atria. Genes Dev. *21*, 1098–1112.

Horsthuis, T., Buermans, H.P., Brons, J.F., Verkerk, A.O., Bakker, M.L., Wakker, V., Clout, D.E., Moorman, A.F., t Hoen, P.A., and Christoffels, V.M. (2009). Gene expression profiling of the forming atrioventricular node using a novel tbx3-based node-specific transgenic reporter. Circ. Res. *105*, 61–69.

Ionta, V., Liang, W., Kim, E.H., Rafie, R., Giacomello, A., Marban, E., and Cho, H.C. (2015). SHOX2 overexpression favors differentiation of embryonic stem cells into cardiac pacemaker cells, improving biological pacing ability. Stem Cell Rep. *4*, 129–142.

Kapoor, N., Liang, W., Marban, E., and Cho, H.C. (2013). Direct conversion of quiescent cardiomyocytes to pacemaker cells by expression of Tbx18. Nat. Biotechnol. *31*, 54–62.

Liang, W., Han, P., Kim, E.H., Mak, J., Zhang, R., Torrente, A.G., Goldhaber, J.I., Marbán, E., and Cho, H.C. (2020). Canonical Wnt signaling promotes pacemaker cell specification of cardiac mesodermal cells derived from mouse and human embryonic stem cells. Stem Cells *38*, 352–368.

Liang, X., Zhang, Q., Cattaneo, P., Zhuang, S., Gong, X., Spann, N.J., Jiang, C., Cao, X., Zhao, X., Zhang, X., et al. (2015). Transcription factor ISL1 is essential for pacemaker development and function. J. Clin. Invest. *125*, 3256–3268.

Luo, X.L., Zhang, P., Liu, X., Huang, S., Rao, S.L., Ding, Q., and Yang, H.T. (2021). Myosin light chain 2 marks differentiating ventricular cardiomyocytes derived from human embryonic stem cells. Pflugers Arch. *473*, 991–1007.

McCarthy, D.J., Campbell, K.R., Lun, A.T., and Wills, Q.F. (2017). Scater: pre-processing, quality control, normalization and visualization of single-cell RNA-seq data in R. Bioinformatics *33*, 1179–1186.

McNally, E.M., and Svensson, E.C. (2009). Setting the pace: tbx3 and Tbx18 in cardiac conduction system development. Circ. Res. *104*, 285–287.

Mond, H.G., and Proclemer, A. (2011). The 11th world survey of cardiac pacing and implantable cardioverter-defibrillators: calendar year 2009–a World Society of Arrhythmia's project. Pacing Clin. Electrophysiol. : PACE *34*, 1013–1027.

Oh, Y., Cho, G.S., Li, Z., Hong, I., Zhu, R., Kim, M.J., Kim, Y.J., Tampakakis, E., Tung, L., Huganir, R., et al. (2016). Functional coupling with cardiac muscle promotes maturation of hPSC-derived sympathetic neurons. Cell Stem Cell *19*, 95–106.

Ortega, F.A., Butera, R.J., Christini, D.J., White, J.A., and Dorval, A.D., 2nd (2014). Dynamic clamp in cardiac and neuronal systems using RTXI. Methods Mol. Biol. *1183*, 327–354.

Patel, Y.A., George, A., Dorval, A.D., White, J.A., Christini, D.J., and Butera, R.J. (2017). Hard real-time closed-loop electrophysiology with the Real-Time eXperiment Interface (RTXI). PLoS Comput. Biol. *13*, e1005430.

Postea, O., and Biel, M. (2011). Exploring HCN channels as novel drug targets. Nat. Rev. Drug Discov. *10*, 903–914.

Protze, S.I., Liu, J., Nussinovitch, U., Ohana, L., Backx, P.H., Gepstein, L., and Keller, G.M. (2017a). Sinoatrial node cardiomyocytes derived from human pluripotent cells function as a biological pacemaker. Nat. Biotechnol. *35*, 56–68.

Protze, S.I., Liu, J., Nussinovitch, U., Ohana, L., Backx, P.H., Gepstein, L., and Keller, G.M. (2017b). Sinoatrial node cardiomyocytes derived from human pluripotent cells function as a biological pacemaker. Nat. Biotechnol. *35*, 56–68.

Ren, J., Han, P., Ma, X., Farah, E.N., Bloomekatz, J., Zeng, X.I., Zhang, R., Swim, M.M., Witty, A.D., Knight, H.G., et al. (2019). Canonical Wnt5b signaling directs outlying Nkx2.5+ mesoderm into pacemaker cardiomyocytes. Dev. Cell *50*, 729–743.e5.

Tchieu, J., Zimmer, B., Fattahi, F., Amin, S., Zeltner, N., Chen, S., and Studer, L. (2017). A modular platform for differentiation of human PSCs into all major ectodermal lineages. Cell Stem Cell *21*, 399–410.e7.

Torrente, A.G., Mesirca, P., Neco, P., Rizzetto, R., Dubel, S., Barrere, C., Sinegger-Brauns, M., Striessnig, J., Richard, S., Nargeot, J., et al. (2016). L-type Cav1.3 channels regulate ryanodine receptor-dependent Ca^{2+} release during sino-atrial node pacemaker activity. Cardiovasc. Res. *109*, 451–461.

Tsai, S.Y., Ghazizadeh, Z., Wang, H.J., Amin, S., Ortega, F.A., Badieyan, Z.S., Hsu, Z.T., Gordillo, M., Kumar, R., Christini, D.J., et al. (2020). A human embryonic stem cell reporter line for monitoring chemical-induced cardiotoxicity. Cardiovasc. Res. *116*, 658–670.

Tucker, N.R., Chaffin, M., Fleming, S.J., Hall, A.W., Parsons, V.A., Bedi, K.C., Jr., Akkad, A.D., Herndon, C.N., Arduini, A., Papangeli, I., et al. (2020). Transcriptional and cellular diversity of the human heart. Circulation *142*, 466–482.

Turbendian, H.K., Gordillo, M., Tsai, S.Y., Lu, J., Kang, G., Liu, T.C., Tang, A., Liu, S., Fishman, G.I., and Evans, T. (2013). GATA factors efficiently direct cardiac fate from embryonic stem cells. Development *140*, 1639–1644.

van Eif, V.W.W., Stefanovic, S., van Duijvenboden, K., Bakker, M., Wakker, V., de Gier-de Vries, C., Zaffran, S., Verkerk, A.O., Boukens, B.J., and Christoffels, V.M. (2019). Transcriptome analysis of mouse and human sinoatrial node cells reveals a conserved genetic program. Development *146*, dev173161.

Vedantham, V., Evangelista, M., Huang, Y., and Srivastava, D. (2013). Spatiotemporal regulation of an Hcn4 enhancer defines a role for Mef2c and

HDACs in cardiac electrical patterning. Dev. Biol. *373*, 149–162.

Vedantham, V., Galang, G., Evangelista, M., Deo, R.C., and Srivastava, D. (2015). RNA sequencing of mouse sinoatrial node reveals an upstream regulatory role for Islet-1 in cardiac pacemaker cells. Circ. Res. *116*, 797–803.

Wang, J., Klysik, E., Sood, S., Johnson, R.L., Wehrens, X.H., and Martin, J.F. (2010). Pitx2 prevents susceptibility to atrial arrhythmias by inhibiting left-sided pacemaker specification. Proc. Natl. Acad. Sci. U S A. *107*, 9753–9758.

Wiese, C., Grieskamp, T., Airik, R., Mommersteeg, M.T., Gardiwal, A., de Gier-de Vries, C., Schuster-Gossler, K., Moorman, A.F., Kispert, A., and Christoffels, V.M. (2009). Formation of the sinus node head and differentiation of sinus node myocardium are independently regulated by Tbx18 and Tbx3. Circ. Res. *104*, 388–397.

Woods, C.E., and Olgin, J. (2014). Atrial fibrillation therapy now and in the future: drugs, biologicals, and ablation. Circ. Res. *114*, 1532–1546.

Ye, W., Wang, J., Song, Y., Yu, D., Sun, C., Liu, C., Chen, F., Zhang, Y., Wang, F., Harvey, R.P., et al. (2015). A common Shox2-Nkx2-5 antagonistic mechanism primes the pacemaker cell fate in the pulmonary vein myocardium and sinoatrial node. Development *142*, 2521–2532.

Yechikov, S., Kao, H.K.J., Chang, C.W., Pretto, D., Zhang, X.D., Sun, Y.H., Smithers, R., Sirish, P., Nolta, J.A., Chan, J.W., et al. (2020). NODAL inhibition promotes differentiation of pacemaker-like cardiomyocytes from human induced pluripotent stem cells. Stem Cell Res. *49*, 102043.

Zeltner, N., Fattahi, F., Dubois, N.C., Saurat, N., Lafaille, F., Shang, L., Zimmer, B., Tchieu, J., Soliman, M.A., Lee, G., et al. (2016). Capturing the biology of disease severity in a PSC-based model of familial dysautonomia. Nat. Med. *22*, 1421–1427.

Zhao, H., Wang, F., Zhang, W., Yang, M., Tang, Y., Wang, X., Zhao, Q., and Huang, C. (2020a). Overexpression of TBX3 in human induced pluripotent stem cells (hiPSCs) increases their differentiation into cardiac pacemaker-like cells. Biomed. Pharmacother. *130*, 110612.

Zhao, M.T., Shao, N.Y., and Garg, V. (2020b). Subtype-specific cardiomyocytes for precision medicine: where are we now? Stem Cells *38*, 822–833.

Zhu, W.Z., Xie, Y., Moyes, K.W., Gold, J.D., Askari, B., and Laflamme, M.A. (2010). Neuregulin/ErbB signaling regulates cardiac subtype specification in differentiating human embryonic stem cells. Circ. Res. *107*, 776–786.

STAR★METHODS

KEY RESOURCES TABLE

REAGENT or RESOURCE	SOURCE	IDENTIFIER
Antibodies		
ISL1	DSHB	#39.4D5 RRID:AB_2314683
GFP	Abcam	# ab13970 RRID:AB_300798
HCN4	Abcam	# ab85023 RRID:AB_2120039
TBX5	Ptglab	# 13178-1-AP RRID:AB_10638435
NKX2.5	Ptglab	# 13921-1-AP RRID:AB_1851479
Cav3.1	Alomone	# ACC-021 RRID:AB_2039779
Cav1.3	Alomone	# ACC-005 RRID:AB_2039775
Cx30.2	Atlas antibodies	# HPA015024 RRID:AB_1847132
Synapsin	Enzo	# ADI-905-782-100 RRID:AB_2039598
Cardiac Troponin	R&D Systems	#ab137346
Cleaved Caspase-3	Cell Signaling 9602S	# NB110-2546 RRID:AB_792426
Donkey anti-Mouse IgG (H+L) Highly Cross-Adsorbed Secondary Antibody, Alexa Fluor 488	Thermo Fisher Scientific	#A-21202 RRID:AB_141607
Alexa Fluor 488 AffiniPure Donkey Anti-Guinea Pig IgG (H+L)	Jackson Immunoresearch Labs	#706-545-148 RRID:AB_2340472
Donkey anti-Mouse IgG (H+L) Highly Cross-Adsorbed Secondary Antibody, Alexa Fluor 594	Thermo Fisher Scientific	#A-21203 RRID:AB_2535789
Donkey anti-Rabbit IgG (H+L) Secondary Antibody, Alexa Fluor 594 conjugate	Thermo Fisher Scientific	#A-21207 RRID:AB_141637
Donkey anti-Rabbit IgG (H+L) Secondary Antibody, Alexa Fluor 647 conjugate	Thermo Fisher Scientific	#A-31573 RRID:AB_2536183
Donkey anti-Mouse IgG (H+L) Secondary Antibody, Alexa Fluor 647	Thermo Fisher Scientific	#A-31571 RRID:AB_162542
Donkey anti-Goat IgG (H+L) Cross-Adsorbed Secondary Antibody, Alexa Fluor 647	Thermo Fisher Scientific	#A-21447 RRID:AB_2535864
Donkey anti-Chicken IgG (H+L) Cross-Adsorbed Secondary Antibody, Alexa Fluor 488	Jackson Immunoresearch Labs	#703-545-155 RRID:AB_2340375
Donkey anti-Sheep IgG (H+L) Cross-Adsorbed Secondary Antibody, Alexa Fluor 647	Thermo Fisher Scientific	#A-21448 RRID:AB_10374882
DAPI	Santa Cruz	#sc-3598
Chemicals, peptides, and recombinant proteins		
Y-27632	MedchemExpress	#HY-10583
CHIR99021	Stem-RD	#13122
Cucurbitacin	Sigma Aldrich	#C4493
SU5402	Tocris	#3300
Retinoic acid	Sigma Aldrich	#R2625-500MG
AG 490	Sigma Aldrich	#T3434

(*Continued on next page*)

Continued

REAGENT or RESOURCE	SOURCE	IDENTIFIER
Chidamide	Selleckchem	#S8567
Doxorubicin Hydrochloride	Sigma Aldrich	#D1515
Physcion	Sigma Aldrich	#17797
XAV939	Tocris	#3748
IWP	Tocris	#3533
IWP2	R&D Systems	#3533/50
Alrestatin	Selleckchem	S5803
Epalrestat	Sigma Aldrich	SML0527
Cayman Epigenetic Chemical library	Cayman	#11076
Prestwick Drug Collection	Prestwick	
Recombinant Human BMP-4 Protein	R & D Systems	#314-BP
Activin A	R&D Systems	#338-AC-500/CF
Deposited data		
RNA-seq	GEO database	GSE118085
scRNA-seq	GEO database	GSE119682
Experimental models: Cell lines		
Human: H9 (WA-09) hESC line	WiCell Research Institute	NIHhESC-10-0062
Human: iPSC line #5	New York Stem Cell Foundation	N/A
Human: iPSC line #33	New York Stem Cell Foundation	N/A
Oligonucleotides		
Primers for hNPPA, hTBX3, hTBX18, hTBX5, hNKX2.5, hISL1, hHCN4, hSHOX2, see Table S2	This paper	N/A
Primers for SHOX2:GFP genotyping, see Table S2	This paper	N/A
Software and algorithms		
Rstudio	Rstudio	https://rstudio.com
Seurat R package v3.1.4	(Butler et al., 2018)	https://satijalab.org/seurat/
Adobe illustrator CC2017	Adobe	https://www.adobe.com/product/photoshop.html
Graphpad Prism 6	Graphpad software	https://www.graphpad.com
Other		
mTeSR1 Complete Kit	Stem Cell Technologies	#85850
Penicillin-Streptomycin	Gibco Thermo Fisher	#15070063
GlutaMAX Supplement	Thermo Fisher Scientific	#35050079
ITS-X	Thermo Fisher Scientific	#51500056
Accutase	Stemcell Technologies	# 07920
ReleSR	Stemcell Technologies	# 05872
B27 minus insulin	Thermo Fisher Scientific	# A1895601
Matrigel	Corning	#354234
N2	Stem Cell Technologies	#7156
B27	Life Technologies	#12587-010
DMEM/F12	Thermo Fisher Scientific	# 10565018
Deposited data		
Single cell RNA-seq	GEO	GSE119682
RNA-seq	GEO	GSE118085

RESOURCE AVAILABILITY

Lead contact

Further information and requests for resources and reagents should be directed to and will be fulfilled by the lead contact, Shuibing Chen (shc2034@med.cornell.edu).

Materials availability

The dual knock-in *SHOX2:GFP; MYH6:mCherry* reporter line will be available under MTA.

Data and code availability

scRNA-seq and RNA-seq data are publicly available from the GEO repository database with accession number GSE119682 (scRNA-seq) and GSE118085 (RNA-seq), respectively.

Code availability: None.

EXPERIMENTAL MODEL AND SUBJECT DETAILS

Cell lines

hESC line H9 (Female) and the derivative (*SHOX2:GFP; MYH6:mCherry*) line, and human iPSC clones (iPSC #5, Female; iPSC #33, Female, New York Stem Cell Foundation)were grown on matrigel-coated plates and maintained in mTeSR medium (Stem Cell Technologies). hESCs and iPSC work has been approved by Tri-SCI ESCRO committee and conforms to the relevant regulatory standards.

METHOD DETAILS

Sinoatrial and ventricular myocyte induction

Differentiation was initiated 72 h after plating when the culture was approximately 80% confluent.

Step 1: Cells were differentiated with 1.5 μM CHIR99021 (CHIR, Stem-RD), 20 ng/mL BMP4 and 20 ng/mL Activin A in RPMI (Cellgro) supplemented with B27 minus insulin, 2 mM GlutaMAX, 1x NEAA and 1x Pen/Strep for 3 days (RB27-INS).

Step 2: For hPSC-V cardiomyocyte differentiation, cells were treated for an additional 3 days with 5 μM XAV939 (Tocris). From day 6 onward, hPSC-V differentiation were carried out in RPMI supplemented with B27, 2 mM GlutaMAX, 1x NEAA and 1x Pen/Strep (RB27+INS). The differentiation efficiency was approximately 85–90% (Tsai et al., 2020).

For hPSC-SAN differentiation, Step 1 was followed by addition of 0.1 μM cucurbitacin (Sigma Aldrich), 1 μM retinoic acid, 5 μM SU5402 (SU, Tocris) in RB27-INS from day 3–6. 5 μM XAV939 was added from day 5–6. From day 6–9, cells were cultured with 5 μM Tyrphostin AG 490 (Sigma Aldrich) in RB27+INS. At day 7–9, 5 μM chidamide was added to the differentiation cocktail. After day 9, hPSC-SAN differentiation was carried out in RPMI supplemented with B27, 2 mM GlutaMAX, 1x NEAA and 1x Pen/Strep (RB27+INS).

FACS and immuno-fluorescence

For FACS analysis, the cells were dissociated with Accutase (Innovative Cell Technologies) for 15 min at 37°C and fixed and permeabilized with the FOXP3 Fixation/Permeabilization set (eBiosciences). Subsequently, they were washed, blocked and permeabilized using FOXP3 permeabilization buffer (eBiosciences) according to the manufacturer's protocol. The cells were stained with primary (overnight 4 degrees) and secondary (45 min, room temperature) antibodies and analyzed using a flow cytometer. For immunofluorescence, cells were fixed with 4% PFA (eBiosciences) for 20 min at room temperature. Next, cells were blocked and permeabilized in 5% horse serum (Invitrogen), 0.3% Triton X in PBS for 1 h at room temperature, followed by primary antibody incubation overnight. After several rounds of washing, secondary antibodies were added for 1 h at room temperature. Nuclei were stained with DAPI. Primary antibodies and working dilutions are listed in Table S3.

Gene expression analysis

Total RNA was isolated using the Qiagen RNeasy mini kit according to manufacturer instructions. cDNA synthesis was performed using TAKARA PrimeScript 1st strand cDNA synthesis kit. qRT-PCR reactions

were generated using Roche SYBR green PCR mix (Roche). Each data point represents at minimum 3 independent biological replicates. Primary antibodies and working dilutions are listed in Table S2.

Generation of the SHOX2:GFP; MYH6:mCherry dual hESC reporter line

The αMHC:mCherry reporter line was created in our previous published studies (Tsai et al., 2020). For targeting the *SHOX2* locus, sgRNA sequences were designed using the website http://crispr.mit.edu/ and targeted the sequence: 5′- GGCGTTGGCGTCACAGACCC-3′. sgRNA was cloned into the PX459 vector (Addgene, plasmid # 42230 (Cong et al., 2013)). For constructing the SHOX2:GFP donor plasmid, the NLS-eGFP (from Tol2kit plasmid), codon optimized P2A, and left and right homology arms (from H9 genomic DNA) were PCR amplified and assembled using the In-Fusion kit (Clontech) and then cloned into the zero-blunt plasmid (Thermo Fischer). H9 hESCs were disassociated into single cells with Accutase for 5-7 min. Cells were electroporated using human stem cell nucleofector kit2 (Lonza, #VPH-5022) according to the manufacturer guidelines. Briefly, 1 million cells were resuspended in 100 μL nucleofector mix to which was added 2 μg CRISPR targeting plasmid and 4 μg donor plasmid. Cells were re-plated on matrigel coated plates with ROCK inhibitor. Two days after electroporation cells were treated with puromycin (0.5 μg/mL) for two days. About two weeks after electroporation individual colonies were picked and expanded for PCR genotyping and sequencing for the reporter lines. Note that both reporter genes are expressed with a self-cleaving sequence and do not generate fusion proteins. The sequences for all primers used for generating the donor plasmids are listed in Table S2.

Bulk RNA sequencing

For RNA sequencing, total RNA was isolated using the Agilent nano kit according to manufacturer instructions. The quality of RNA samples was examined using an Agilent bioanalyzer. cDNA libraries were generated using TruSeq RNA Sample Preparation (Illumina). Each library was sequenced using a single-read 50 bp in HiSeq4000 (Illumina). Gene expression levels were analyzed with TopHat and Cufflinks by the Weill Cornell Genomic Core facility. Raw data were normalized to that from SHOX2:GFP negative cells to define fold-change. Gene lists were filtered based on expression level differences ≥ 4 or ≤ -4. Murine sinoatrial and atrial tissues were obtained from a published database (GSE65658). False discovery rate (FDR) q values <0.25 or nominal (NOM) p values <0.05 were considered significant. The expression data were normalized for each gene by subtracting their mean across samples and then dividing by their standard deviation. The normalization was performed separately on three sets of samples (D25 samples, D40 samples and public samples) to remove batch effects introduced by experiments. The heatmap plot was generated using heatmap.2 in the R "gplots" package.

Single cell RNA sequencing

Cells were differentiated into hESC-SAN or cardiomyocyte (V-cell) lineages. hESC-SAN cells were sorted based on GFP, while hPSC-V cells were sorted based on mCherry. Single-cells were captured using a Drop-Seq system. The two aqueous suspensions - the single-cell suspension and the barcoded primer beads suspended in a lysis buffer, were loaded into 3 mL plastic syringes (BD) respectively. Droplet generation oil (BioRad) was loaded into a 10 mL plastic syringe (BD). The three syringes were connected to a 125 μm co-flow device by 0.38 mm inner-diameter polyethylene tubing (Scientific Commodities, Inc.), and injected using syringe pumps (KD Scientific), resulting in ~125 μm emulsion drops with a volume of ~1 nL each. The flow was monitored under an inverted microscope. Droplets were collected in 50 mL falcon tubes; the collection tube was changed out after every 1 mL of combined aqueous flow volume. During droplet generation, the beads were kept in suspension by continuous, gentle magnetic stirring (V&P Scientific). The uniformity in droplet size and the occupancy of beads were evaluated by observing aliquots of droplets under the microscope. The oil from the bottom of each aliquot of droplets was removed after which 30 mL 6X SSC (Life Technologies) at room temperature was added. Collected droplets were broken by adding perfluorooctanol in 30 mL 6X SSC to destabilize the oil-water interface and the microparticles were disrupted. RNA-hybridized beads were extracted. The extracted beads were then washed and resuspended in a reverse transcriptase mix, followed by a treatment with exonuclease I to remove unhybridized, non-extended primers. The beads were then washed, counted, and aliquoted into PCR tubes for PCR amplification. 15-18 cycles of PCR amplification were applied to reach cDNA concentration at 400-1000 pg/μL after pre-PCR test step. The final PCR products were purified and pooled, and the amplified cDNA quantified on an Agilent 2100 BioAnalyzer High Sensitivity Chip. The cDNA was fragmented and amplified for sequencing with the Nextera XT DNA sample prep kit (Illumina) using custom primers. The libraries were purified, quantified, and sequenced on the Illumina NextSeq 500 at > 50,000 reads/cell.

After quality assessment of the sequencing with FastQC v0.11.3 (http://www.bioinformatics.babraham.ac.uk/projects/fastqc/), all single-cell RNA-seq samples were processed according to the Drop-seq Computational Protocol with the Drop-seq Toolkit v1.2 created by the McCarroll Lab(http://mccarrolllab.com/dropseq/). Sequences were first tagged with their corresponding cell and molecular barcodes (unique molecular identifiers, UMI) using dropseq TagBamWithReadSequenceExtended. Cell and molecular barcodes were required to have a minimum base quality of 10 across their lengths, otherwise they were discarded. SMART adapter sequences were trimmed from the 5′ end of each read whenever there were at least five continuous bases exactly matching the SMART adapter (dropseq TrimStartingSequence). Putative poly(A) tails were trimmed from the 3′ end whenever there were stretches of at least 6 adenosines with zero mismatches (dropseq PolyATrimmer). The UMI-tagged and trimmed reads were then aligned with default parameters to the human reference genome (GRCh38) using STAR (v2.4.2a)(Dobin et al., 2013). The final file containing alignment information plus the cell and UMI tags was generated with Picard MergeBamAlignment and Picard MergeBamAlignment. Sequences that mapped to more than one locus were excluded from further analysis by filtering reads with a mapping quality lower than 10.

To determine the numbers of detected transcripts per gene and cell, the overlaps of the aligned reads with gene annotation (Ensembl release 76) were counted and summarized using dropseq TagReadWith GeneExon and dropseq DigitalExpression. Individual gene expression matrices from each sample were combined in R to create a single gene count matrix for all cells and genes.

The count matrix was read into R; basic quality metrics such as the distributions of the numbers of gene counts per cell and gene were determined using in-house scripts and the Scater package (McCarthy et al., 2017). We excluded cells with fewer than 100 UMI or fewer than 200 genes per cell, and more than 15% of the UMI mapping to mitochondrial genes. This resulted in 1,571 GFP-negative and 2,057 GFP-positive cells (representing about equal numbers per technical replicate). After filtering the cells, we excluded genes that were expressed in fewer than 5 cells per condition. Additionally, genes had to be covered by at least 10 UMI across all cells of the same condition. 13,448 genes met these filtering criteria and were used for downstream analyses. The UMI counts were adjusted for the differences in the individual cell coverage by dividing every gene count by the total number of UMI counts of the respective cell (library size) and multiplying with the median of all library sizes. These scaled UMI counts were then further de-noised using the MAGIC algorithm. All expression values shown in the manuscript are log10-transformed values (with an offset of 0.01 to avoid taking the log of zeros) after applying MAGIC(https://doi.org/10.1101/111591). t-SNE was performed with the Rtsne package(https://github.com/jkrijthe/Rtsne). Hierarchical clustering was applied to all cells and a subset of genes and visualized with the pheatmap function(https://CRAN.R-project.org/package=pheatmap). Genes and cells were clustered with the base R hclust function using Euclidean distances and the agglomeration function ''complete''.

Adult heart single cell analysis

We used an existing single cell RNA-seq dataset generated from heart tissue biopsies of adult healthy individuals (Tucker et al., 2020). Briefly, cells with poor quality were removed if 1) they had less than 100 genes or greater than predefined upper outlier cutoff, 2) the number of UMI for the cell was greater than predicted upper outlier cutoff, or 3) the percentage of mitochondrial gene content was greater than 5%. Please refer to the original manuscript for detailed information about the cutoffs.

Data normalization, variable gene identification and data scaling was done using Seurat V3. During data scaling, variability due to read coverage (nCount_RNA), cell cycle effects (S.Score and G2M.score) and the percentage of mitochondrial and ribosomal gene reads were regressed out. The Seurat featureplot and Dotplot functions were used to visualize genes of interest, and the uniform manifold approximation and projection (UMAP) coordinates provided by the original authors were used for featureplot visualizations.

Clusters 0 to 16 corresponds to 0) Adipocyte; 1) Atrial Cardiomyocyte; 2) Cytoplasmic Cardiomyocyte I; 3) Cytoplasmic Cardiomyocyte II; 4) Endothelium I; 5) Endothelium II; 6) Fibroblast I; 7) Fibroblast II; 8) Fibroblast III; 9) Lymphocyte; 10) Macrophage; 11) Neuronal; 12) Pericyte; 13) Vascular smooth muscle; 14) Ventricular Cardiomyocyte I; 15) Ventricular Cardiomyocyte II; and 16) Ventricular Cardiomyocyte III.

Calcium imaging

hESC-derived cells were plated on ibidi plates coated with gelatin. The cells were loaded with 2 μM Fluo-4 AM dissolved in 1:1 (v/v) of 20% Pluronic®-F127 and DMSO with stock concentration of 1 mM for 45 min at RT in Tyrode solution consisting of: 140 mM NaCl, 5.4 mM KCl, 1 mM $MgCl_2$, 1.8 mM $CaCl_2$, 10 mM glucose and 10 mM HEPES at pH 7.4. Calcium transients of hESC-derived beating cardiac clusters were recorded on a heated stage using a confocal scanning microscope (Zeiss LSM 710) at intervals of 200 ms (5 frames per second). They were then quantified as the background subtracted fluorescence intensity changes normalized to the background subtracted baseline fluorescence using MetaXpress software. For the experiments involving drug treatment (Isoproterenol 1 μM, Carbachol 5 μM and Ivabradine 1 μM), the cells were treated with either vehicle or drug and the imaging was performed within 10 s (for Isoproterenol and Carbachol) or 5 min (Ivabradine) of adding the drug.

Cellular electrophysiology and characterization

Spontaneous action potentials were recorded over 10 s with the perforated patch clamp technique using an AM-Systems (WA, USA) model 2400 amplifier in current-clamp mode and the software platform Real-Time eXperiment Interface (RTXI; www.rtxi.org) (Ortega et al., 2014; Patel et al., 2017). Cells were superfused at 35°C with a Tyrode's solution containing in mM: 137 NaCl, 5.4 KCl, 2 CaCl2, 1 MgSO4, 10 HEPES, and 10 glucose at pH 7.35 (NaOH). Whole cell access was achieved using 480 μg/mL Amphotericin-B (Sigma-Aldrich, MO, USA) in a pipette solution also containing in mM: 5 NaCl, 20 KCl, 120 K-aspartate, and 10 HEPES at pH 7.2 (KOH). A liquid junction potential of 14 mV was corrected. Pipettes were pulled from 1.5 mm capillary tubes (AM-Systems, WA, USA) to a resistance between 2.5 – 3.5 MΩ. Cells were characterized as nodal-like if they exhibited spontaneity and a slow upstroke (dV/dt_{max} < 30 V/s). hESC-V voltage recordings were used for comparison (Tsai et al., 2020).

Whole-cell currents were recorded with an extracellular solution containing (mM) 140 NaCl, 5.4 KCl, 1.8 $CaCl_2$, 1 $MgCl_2$, 10 glucose, and 10 HEPES, *p*H 7.4. Borosilicate glass patch pipettes (resistance 1.5–2.5 MΩ) were filled with internal solution containing (mM): 125 K-gluconate, 20 KCl, 5 NaCl, 1 $MgCl_2$, 5 MgATP, and 10 HEPES, with pH adjusted to 7.2 with KOH. All chemicals were from Sigma-Aldrich. The signal was filtered at 5 Hz. The liquid junction potentials were not corrected. Data are presented as mean ± SEM.

Chemical screen

The epigenetic library was purchased from Cayman Chemicals (Item №. 11076). The Epigenetics Screening Library contains compounds that modulate the activity of methyltransferases, demethylases, histone acetyltransferases, histone deacetylases, and acetylated histone binding proteins. The dual-reporter hESC line was differentiated into mesoderm lineage by adding Activin, BMP4 and CHIR99021 to the differentiation medium for 3 days and then switched to differentiation medium containing Retinoic Acid, Cucurbitacin, and SU5402 for another 3 days. After 6 days, the cells were replated into 384 well plates and the medium was changed to RPMI+ complete B27 containing Tyrphostin AG490. After 24 h, small molecules from the chemical library were added to the media and incubated for 48 h. The medium was changed to RPMI plus complete B27 on day 9 and it was changed every 48 h afterwards. Cells were imaged using a high content imaging system on day 14 and assessed for GFP percentage. The compound with least toxicity and highest percentage of GFP was selected as potential epigenetic modulator compound to enhance differentiation of sinoatrial nodal cells.

QUANTIFICATION AND STATISTICAL ANALYSIS

N = 3 independent biological replicates were used for all experiments unless otherwise indicated. n.s. indicates a non-significant difference. p-values were calculated by unpaired two-tailed Student's t-test or one-way ANOVA test unless otherwise indicated. *$p < 0.05$, **$p < 0.01$ and ***$p < 0.001$. Data are represented as mean ± SEM.